Light: Science & Applications (2013) 2, e66; doi:10.1038/lsa.2013.22

www.nature.com/lsa

ORIGINAL ARTICLE

Plasmonics for solid-state lighting: enhanced excitation and directional emission of highly efficient light sources

Gabriel Lozano[1], Davy J Louwers[2], Said RK Rodríguez[1], Shunsuke Murai[1,3], Olaf TA Jansen[2], Marc A Verschuuren[2] and Jaime Gómez Rivas[1,4]

Light sources based on reliable and energy-efficient light-emitting diodes (LEDs) are instrumental in the development of solid-state lighting (SSL). Most research efforts in SSL have focused on improving both the intrinsic quantum efficiency (QE) and the stability of light emitters. For this reason, it is broadly accepted that with the advent of highly efficient (QE close to 1) and stable emitters, the fundamental research phase of SSL is coming to an end. In this study, we demonstrate a very large improvement in SSL emission (above 70-fold directional enhancement for p-polarized emission and 60-fold enhancement for unpolarized emission) using nanophotonic structures. This is attained by coupling emitters with very high QE to collective plasmonic resonances in periodic arrays of aluminum nanoantennas. Our results open a new path for fundamental and applied research in SSL in which plasmonic nanostructures are able to mold the spectral and angular distribution of the emission with unprecedented precision.
Light: Science & Applications (2013) **2,** e66; doi:10.1038/lsa.2013.22; published online 10 May 2013

Keywords: diffraction; fluorescence; LED; nanophotonics; plasmonics

INTRODUCTION

Light-emitting diode (LED) technology is reaching the maturity phase necessary to replace the more than 100-year-old technology of incandescent lamps. It has been said that LED-based sources will light up the world.[1] During the past 10 years, developments in materials have opened the door for white LEDs, in which several wavelengths combine to mimic the solar spectrum. Following the classification presented by Pimputkar *et al.*,[1] there are two main routes to achieving white light using LEDs. The first is to mix the light from individual electrically driven LEDs that emit the primary colors, i.e., red, green and blue.[2] The current absence of high-efficiency green LEDs limits the applicability of this approach to the generation of white light.[3] The second and more extended path consists in using a material, usually known as 'phosphor', which absorbs a significant fraction of the light emitted by an electrically driven ultraviolet or blue LED and re-emits at a longer wavelength. Mixing the non-absorbed blue light with the emission provides a spectrum that is perceived as white by the human eye.[4] Most of the research on solid-state lighting (SSL) has, thus far, focused on the development of light emitters with high internal quantum efficiency (QE)[5] and light extraction mechanisms using dielectric structures[6] to meet the requirements for general illumination applications. Although SSL sources are efficient, their angular emission profiles are usually Lambertian. Depending on the application, this may result in the need for secondary optics, which are frequently bulky and lossy and degrade the total system efficiency.

Metallic nanoparticles provide unique ways of manipulating light at length scales smaller than the wavelength. These nanostructures are known as optical antennas or nanoantennas because of their resonant behavior at optical frequencies, which can be tuned by varying their sizes and shapes.[7–11] This behavior is achieved through the excitation of surface plasmons, which are strong optical resonances based on coherent oscillations of the free electrons in the metal nanoparticles, driven by the electric field of light.[12] In recent years, the field of surface plasmon polariton optics or plasmonics has shifted from a domain in which fundamental insights were developed into a discipline that has become relevant to applications.[13] However, to date, no cutting-edge applications of plasmonic structures are able to compete with state-of-the-art SSL technologies. One major problem of metals is the inherent losses associated with their conductivity. In the specific case of light emission, plasmonic resonances' ability to enhance the fluorescence of nearby emitters depends strongly on the efficiency of the emitter and on its location in respect to the metal/dielectric interface.[14] The lower the QE, the higher the enhancement factor that can be achieved using plasmonic nanostructures.[15–19] For high QE emitters, losses in the metal lead to a reduction of this efficiency, limiting the enhancement factor.[18,20–22] To minimize this effect, most researchers use noble metals such as gold or silver, as these metals support localized surface plasmon resonances and exhibit the lowest damping. A major disadvantage is that these materials are expensive and difficult to process. Moreover, local field enhancements associated with localized surface

[1]Center for Nanophotonics, FOM Institute AMOLF, c/o Philips Research Laboratories, Eindhoven, The Netherlands; [2]Philips Research Laboratories, Eindhoven, The Netherlands; [3]Department of Material Chemistry, Graduate School of Engineering, Kyoto University, Kyoto, Japan and [4]COBRA Research Institute, Eindhoven University of Technology, Eindhoven, The Netherlands
Correspondence: Dr G Lozano, Center for Nanophotonics, FOM Institute AMOLF, c/o Philips Research Laboratories, High Tech Campus 4, 5656 AE, Eindhoven, The Netherlands
E-mail: lozano@amolf.nl
Or Professor J Gómez-Rivas, Center for Nanophotonics, FOM Institute AMOLF, c/o Philips Research Laboratories, High Tech Campus 4, 5656 AE, Eindhoven, The Netherlands
E-mail: rivas@amolf.nl
Received 10 August 2012; revised 20 December 2012; accepted 24 December 2012

plasmon resonances lie on near-field interactions that extend only a few tens of nanometers away from the metal surface. Therefore, almost no benefit can be attained using localized resonances when dealing with highly efficient emitters distributed over large volumes, such as those that are interesting for use in lighting applications.[23,24]

In this article, we demonstrate how plasmonics can enhance the performance of close-to-one QE dyes employed in SSL. In contrast to the previous studies investigating emitters and metallic structures, we focus here on improving the emission of already efficient emitters beyond the limit imposed by near-field effects. We make use of arrays of metallic nanoantennas that sustain collective plasmonic resonances. This allows us to shape the angular pattern of the emission, beaming most of the light into a very narrow angular range in a defined direction. We have investigated the emission characteristics of the plasmonic array using a laser and a Lambertian-like standard LED as sources of blue light. A 60-fold unpolarized emission enhancement compared with a planar layer of dye molecules of similar thicknesses is achieved in the forward direction at a certain emission energy when using a collimated laser source. This enhancement reaches a factor of 70 for p-polarized emission. The integrated enhancement over the emission spectrum of the dye reaches a factor of 14 in the forward direction. In the case of LED excitation, despite the total enhancement factor being reduced, the high directionality of the emission remains unaltered with a 20-fold enhancement in a direction close to the normal. This directional enhancement is explained as the combination of an increased efficiency in the excitation of the dye and an enhanced spatial coherence, which is accomplished by coupling this dye to extended plasmonic modes in the array, and the subsequent out-coupling to free-space radiation. We have realized large periodic arrays of aluminum particles using an imprint lithography technique, which allows the inexpensive and high-quality fabrication of plasmonic structures over large areas. Nanoplasmonics, therefore, offers a new platform on which to develop the next generation of SSL devices.

MATERIALS AND METHODS

Sample fabrication

A schematic of the investigated structure is presented in Figure 1a, and a scanning electron micrograph of the aluminum particles arranged in a square lattice is displayed in Figure 1b. Aluminum is a non-noble, inexpensive metal that presents low absorption losses at visible frequencies and has good heat-dissipation properties. Furthermore, it is a non-toxic, corrosion-resistant and lightweight material. The aluminum nanoantenna arrays were fabricated by substrate conformal imprint lithography in combination with reactive ion etching onto a fused silica substrate.[25] The combination of aluminum and an imprint lithography technology allows the high-quality fabrication of plasmonic patterns with nanometer resolutions. This technology is ready to be applied to a large area using standard inexpensive processes, as has quite recently been demonstrated in the field of photovoltaics.[26] Polymers, appropriately doped with dye molecules and emitting in the visible part of the spectrum, provide stable sources of light for the large-area SSL. The absorbance and photoluminescence (PL) spectra of the dye employed in this investigation (Lumogen F Red 305, BASF) are presented in Figure 1c. This dye is well suited to SSL applications because of its bright PL in the visible spectrum with a very high QE in a polymer matrix (~99% at a very low concentration forming a thin layer, ~85% at 3 wt-%) and good stability. A 10 cm×10 cm plasmonic structure was made of slightly tapered cylindrical aluminum particles, D=140 nm in diameter and h=150 nm in height, arranged in a square array with the lattice constant a=400 nm. A d=650 nm-thick

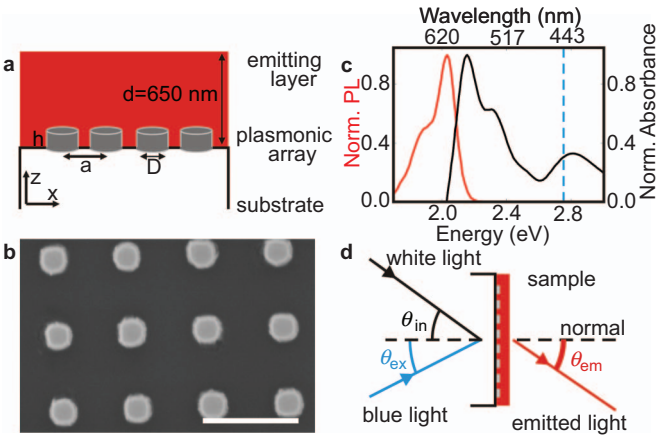

Figure 1 (**a**) Sketch of the sample consisting of a thick layer of fused silica (substrate), a periodic array of aluminum particles (plasmonic array) and a layer of dye molecules embedded in polystyrene (emitting layer). (**b**) Top view of a scanning electron micrograph of aluminum particles arranged in an ordered periodic lattice. Scale bar indicates 500 nm. (**c**) Normalized photoluminescence (red curve) and normalized absorbance (black curve) spectra of the dye (Lumogen F Red 305, BASF). (**d**) Scheme depicting the different angles involved in the experiments. PL, photoluminescence.

polystyrene layer containing dye molecules at a concentration of 3 wt-% was applied over the array by spin coating.

Optical measurements

The variable angle extinction and photoluminescence directional enhancement (PLDE) spectra of the luminescent structure were measured. The extinction is defined as $1-T_0$, with T_0 being the zero-order transmittance normalized by the transmittance through the fused silica substrate and a polystyrene/dye layer. The PLDE is defined for each angle of emission as the PL of the dye layer on top of the array of aluminum particles normalized by the emission of the same layer on top of the flat substrate. The PLDE is, therefore, the most relevant quantity in this investigation, representing the improvement to the light emission introduced by the plasmonic structure. To measure the optical extinction of the plasmonic structure, a collimated beam of light from a halogen lamp illuminated the sample, which was rotated by an angle θ_{in} with respect to the normal around the x-axis while keeping a fiber-coupled spectrometer fixed in the forward direction. For the PLDE measurements, the red dye was excited at a power level far below saturation using blue light (2.76 eV, 450 nm) from either a multimode continuous wave laser 0.01 eV (2 nm) full-width half-maximum or a high-power blue standard LED (full-width half-maximum=0.1 eV) characterized by a Lambertian-like emission pattern 5 cm behind the sample. The emission was collected using a fiber-coupled spectrometer, which was rotated by an angle θ_{em} with respect to the normal toward the sample (see Figure 1d for a schematic representation of the set-up).

Finite-difference time-domain (FDTD) numerical simulations

A three-dimensional FDTD model was set up with Bloch boundary conditions on the horizontal edges and PML-absorbing boundaries on the vertical edges. The dispersion of the metal is fitted using a Drude model. The incident fields are broadband constant transverse wavenumber pulses. The spectra are obtained using Fourier transforms of the time-domain near-field responses that are normalized to the incident pulse.

doi:10.1038/lsa.2013.22

Lifetime measurements

A series of fluorescent lifetime measurements was conducted using a streak camera (Hamamatsu 5680) synchronized with a femtosecond laser (Spectraphysics Tsunami). A pulse-picker and a second harmonic generator (Spectraphysics 3980) were used to enable the excitation of the dye with 2.76 eV pulses at a 2 MHz repetition rate.

RESULTS AND DISCUSSION

Figure 2a presents the measured p-polarized extinction of the investigated structure as a function of the energy of the incident radiation and the angle that forms the incident wave-vector with the normal toward the sample (θ_{in}). The PLDE measurements are displayed as a function of the photon energy of the p-polarized emitted radiation and the emission angle θ_{em} in Figure 2b. All the features observed in PLDE are correlated with those shown in the extinction measurements. Most of the dispersive features observed in the experiment can be associated with electromagnetic surface modes supported by periodic metallic structures.[27] They appear as narrow bands of high extinction that follow the dispersion of the Rayleigh anomalies, i.e., the energy at which a diffracted order radiates in the plane of the array; these bands are known as surface lattice resonances (SLRs).[28–33] SLRs are, therefore, the result of the enhanced radiative coupling of localized surface plasmon polaritons in the individual particles by means of in-plane diffracted orders. SLRs can be described as quasi-bounded surface modes in the array and have a propagation length of several unit cells.[34] From the conservation of the parallel component of the wave-vector at the surface of the array, we have $\pm k_{\|d} = k_{\|i} \pm \mathbf{G}$, where $\pm k_{\|d}$ and $k_{\|i}$ are the parallel components of the diffracted and incident wave vectors, respectively; $\mathbf{G} = (G_x, G_y) = [(2\pi/a)p, (2\pi/a)q]$ is a reciprocal lattice vector; and p and q are the pair of integers defining a diffracted order. Rayleigh anomalies of beams diffracted by the square array of particles are plotted as colored curves in Figure 2a and 2b. They correspond to the onset of $(\pm 1,0)$ and $(0,\pm 1)$ diffracted orders, calculated assuming that the array is embedded in a homogeneous medium, with refractive indexes of 1.47 (gray curves), 1.52 (purple curve) or 1.55 (green curves). These values are obtained by fitting the Rayleigh anomalies to the maxima in the extinction spectrum, measured at $\theta_{in}=0°$. In these experiments, the particle array is not homogenously surrounded by the same dielectric. The particles are on a fused silica substrate with a lower refractive index (1.46) than the polystyrene layer (1.59), which has a finite thickness of 650 nm. Numerical simulations reveal that the different refractive index layers surrounding the array and the finite thickness of the polymer layer modify the distribution of the local field intensities around the particles (see Supplementary Information). The intensity extends farther into the substrate for the resonance at 2.11 eV than for the resonances

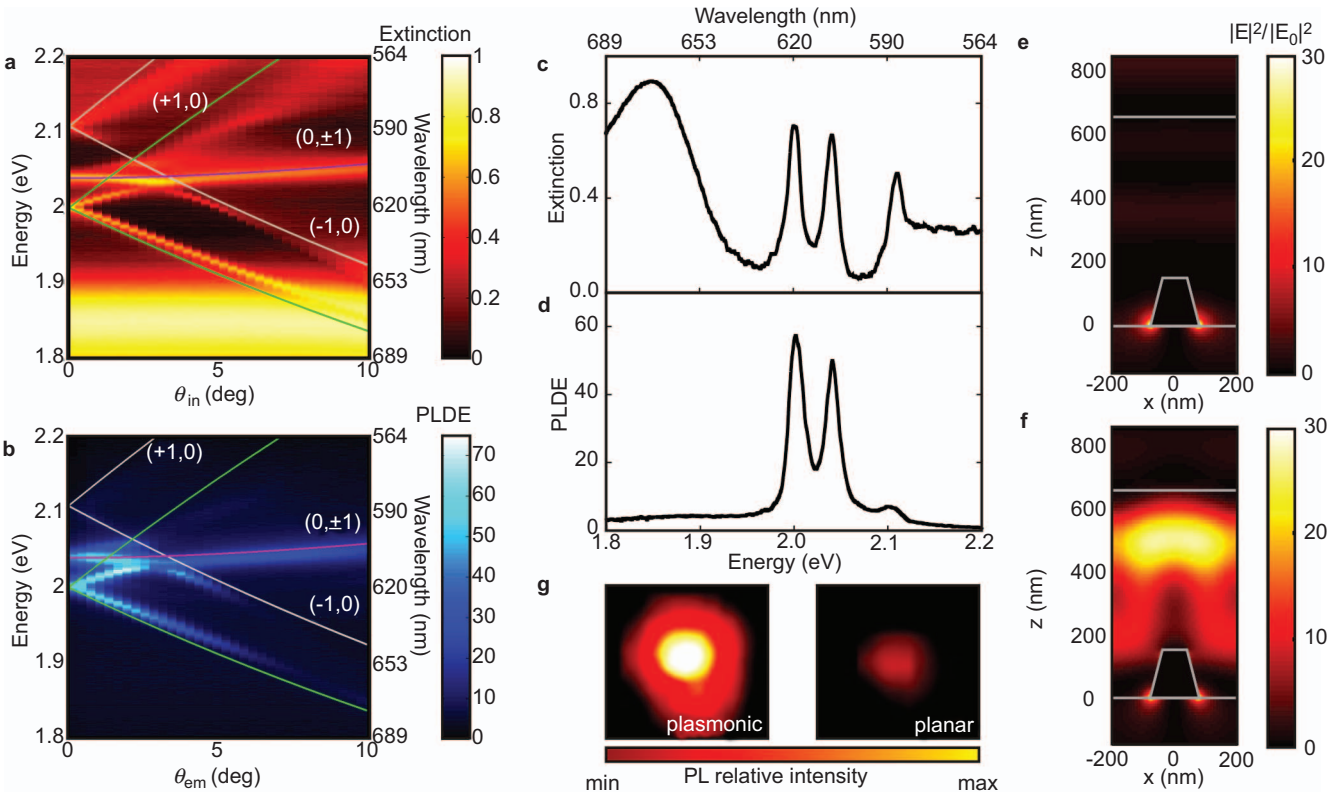

Figure 2 (**a**) Extinction of p-polarized light as a function of the photon energy and the angle of incidence θ_{in} of a layer of dye deposited on top of the investigated array of aluminum particles. (**b**) p-polarized directional emission enhancement as a function of the photon energy and the emission angle θ_{em} measured on the same structure excited with a 2.76 eV continuous wave laser at $\theta_{ex}=0°$. Gray, purple and green curves correspond to the Raleigh anomalies calculated for the beams diffracted in a medium with refractive indexes of 1.47, 1.52 and 1.55, respectively. (**c**) Extinction and (**d**) PLDE as a function of photon energy measured at $\theta_{in}=0°$ and $\theta_{em}=0°$. (**e**, **f**) Simulated spatial distribution of the near-field intensity enhancement in a plasmonic array of antennas on a substrate covered by a polymer layer. The color plot indicates the intensity enhancement of the plane intersecting the antennas at $y=0$ in a unit cell of the array. The simulations consider a plane wave incident normal to the array with a photon energy of (**e**) 1.85 eV and (**f**) 2.04 eV. The antenna and the different dielectric interfaces are outlined using gray curves. (**g**) Digital photographs taken from the unpolarized emission from the dye layer deposited on top of the plasmonic structure (left) and from the same layer deposited on a dielectric substrate (right) at θ_{em} of ~0°. PLDE, photoluminescence directional enhancement.

at 2.04 eV and 2.00 eV, whose field intensities are primarily concentrated in the dye-doped layer. The difference in field intensity distribution causes a difference in the effective refractive index of these modes and the concomitant energy shift. The blue-shift of the 2.11 eV mode is consistent with its higher field intensity in the lower refractive index substrate compared to the modes observed at 2.04 eV and 2.00 eV. It should be noted that this multilayer structure can support index-guided modes coupled to free-space radiation by the array of nanoparticles and, consequently, with a similar dispersion to the SLRs. For simplicity, we have limited the analysis of the extinction and luminescence measurements to SLRs in homogeneous media in which index-guided modes do not exist.

SLRs can couple very efficiently to radiation because of their hybrid plasmonic–photonic characters. Excited emitters in the proximity of the array can decay into SLRs, which radiate into free space, enabling the control of the spontaneous emission.[29,35] We would like to note that similar results may be attained using dielectrics with tailor-made polarizability, as suggested by previous theoretical investigations regarding titania nanoparticles arranged in one-dimensional arrays.[36] In particular, the bands of maximum PLDE follow the dispersion of the SLRs associated with the $(-1,0)$ and $(0,\pm1)$ diffractive orders. Figure 2b shows that a many-fold enhancement of the fluorescence takes place on the narrow bands between $\theta_{em}=0^{\circ}$ and $\theta_{em}=10^{\circ}$. We achieve a maximum PLDE of 72 times at $\theta_{em}=1.5^{\circ}$ and 2.01 eV. Comparable features and enhancement values can be observed for s-polarized emission because of the square symmetry of the array (see Supplementary Information). This remarkable enhancement of the emission occurs close to the normal with respect to the surface. The enhanced and directional emission of the emitters, which are already close to unity efficiency, demonstrates that arrays of nanoparticles can be integrated into lighting devices as efficient and compact secondary collimating optics. Moreover, the ability to tune the dispersion of SLRs by varying the shape and dimensions of the nanoparticles, the lattice structure and the period of the array opens the possibility of fully controlling the emission of the different light emitters integrated in plasmonic-based LEDs. This demonstration of the PLDE of highly efficient emitters contradicts the idea that plasmonic structures are detrimental to the performance of devices using high QE emitters because of inherent Ohmic losses in metals.[37–39] To facilitate further investigation of how the plasmonic array enhances and shapes, the fluorescence of the emitting layer, cuts of the spectra presented in Figure 2a and 2b at $\theta=0^{\circ}$ are displayed in Figure 2c and 2d. Two types of resonances with different line widths can be observed in the measured extinction spectrum: (i) a broad resonance centered at 1.85 eV, which is attributed to localized surface plasmons in individual particles and (ii) three narrow peaks at 2.00 eV, 2.04 eV and 2.11 eV, associated with collective lattice modes. Note that the luminescence is significantly enhanced only at these narrow resonances. Specifically, the solid black curve in Figure 2d depicts three peaks, corresponding to 58-fold, 50-fold and 7-fold PLDEs. It is noteworthy that the localized character of the broad resonance centered at 1.85 eV merely leads to a weak PLDE factor of 4.

To further describe the origin of the spectral features associated with the different plasmonic resonances, in Figure 2e and 2f, we perform numerical three-dimensional FDTD simulations of the spatial distribution of the total electric field intensity enhancement—i.e., near-field intensity normalized by the incident intensity—at two different frequencies: 1.85 eV and 2.04 eV, respectively. The simulated extinction at $\theta_{in}=0^{\circ}$ and the near-field intensity of the resonances at 2.00 eV and 2.11 eV are provided in the Supplementary Information. We consider a plane wave incident to be normal to the array. A small tapering of the aluminum particles was included in the model to account for their actual shapes. The simulation in Figure 2e, which depicts a side view (see Supplementary Information for a top view) of a unit cell of the array, indicates that the broad extinction peak corresponds to an in-plane dipolar resonance. The field is primarily enhanced in the proximity of the particles, as expected for a localized surface plasmon polariton. A major drawback inherent to the use of localized surface plasmon resonances to enhance light-matter interactions is that the emitters need to be accurately positioned with nanometric precision in the region in which the largest electromagnetic enhancement occurs.[17] This characteristic, together with the fact that dye layer extends over a thickness of 650 nm on top of the particle array, leads to the weak PLDE associated with the localized surface plasmon resonance. In contrast, the narrow extinction peak at 2.04 eV corresponds with the collective plasmonic mode associated to the SLR. The field enhancement of this resonance, as shown in Figure 2f, extends over a much larger distance in the space between the nanoantennas,[32] leading to the enhancement of the dye emission from larger volumes. This enhanced emission from large volumes is critical for real SSL applications in which a specific fluorescence count rate must be reached.

To present a clear visual effect of the enormous PLDE attained when using an array of nanoparticles, Figure 2g shows images, taken with a digital camera, of the unpolarized emission from a dye layer deposited onto a flat dielectric substrate, labeled 'planar', compared with the emission from a similar layer but coupled to an array of metallic particles, labeled 'plasmonic'. The former refers to the common configuration used in LED devices.[40] From this point on, we will present the results for the unpolarized emission, as polarization dependency is generally undesirable in SSL devices.

The total PLDE is the result of phenomena taking place at the excitation and emission frequencies of the dye. On the one hand, the absorption efficiency of the dye can be increased by a resonant enhancement at the excitation frequency when the system is optically pumped. On the other hand, in a plasmonic system, the emission is influenced by the modified local density of the optical states and by the out-coupling of the emission to free space.[41,42] To investigate the contribution of the resonant pump enhancement, we have measured the PLDE spectra for unpolarized emission as a function of the excitation angle, fixing the detector at $\theta_{em}=55^{\circ}$, i.e., at an angle at which no plasmonic resonance occurs at the emission frequency. Figure 3a displays the PLDE integrated between 1.75 eV and 2.15 eV as a function of θ_{ex}, showing a ~sixfold overall fluorescence enhancement when the dye molecules are excited at $\theta_{ex}=0^{\circ}$. This enhancement is halved when θ_{ex} is 10°. As noted in the Supplementary Information, the relative contribution of the pump enhancement attained at a different θ_{ex} from the PLDE is roughly proportional to how much blue light is extinct as a function of θ_{in}. The large enhancement at normal incidence is attributed to a higher order SLR and, in particular, to that associated with the $(-1,1)$ diffracted order. As discussed below and in view of the numerical simulations and PL lifetime measurements, this ~sixfold enhancement can primarily be attributed to a resonant enhancement of the excitation of the dye at the frequency of the pump.

Three-dimensional FDTD simulations of the PLDE were performed to separate the contribution of the emission from that of the pump. According to the reciprocity theorem and assuming a set of isotropically oriented dipoles, the PLDE is obtained as the ratio of the integrated electric near-field intensity in a unit cell, computed in a structure with and without metallic particles and calculated for a plane wave illumination along the angle of emission at which the PLDE is

doi:10.1038/lsa.2013.22

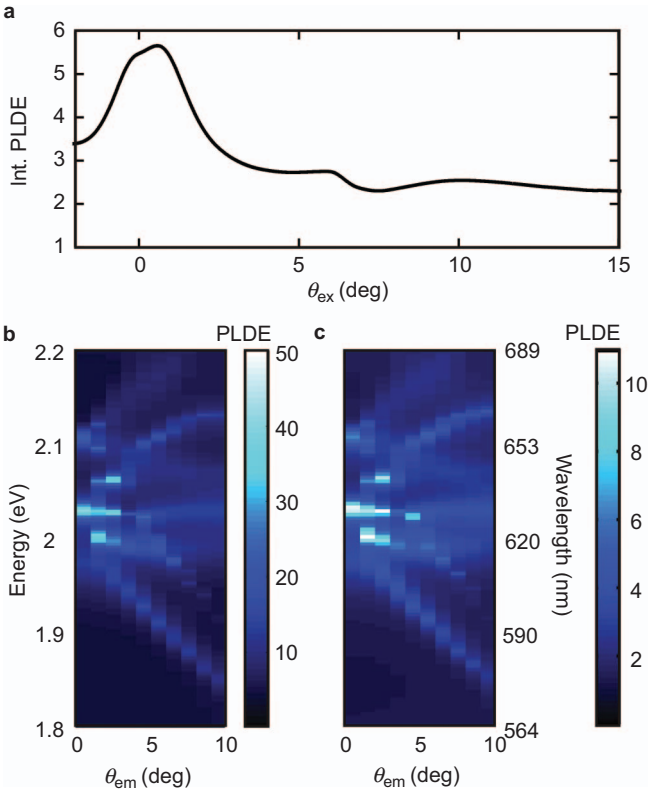

Figure 3 (**a**) PLDE integrated between 1.75 eV and 2.15 eV as a function of the excitation angle when the detector is fixed at θ_{em}=55°. (**b**, **c**) Calculated PLDE using FDTD as a function of energy and θ_{em}, with and without the consideration of resonant excitation at the pump frequency, respectively. FDTD, finite-difference time-domain; PLDE, photoluminescence directional enhancement.

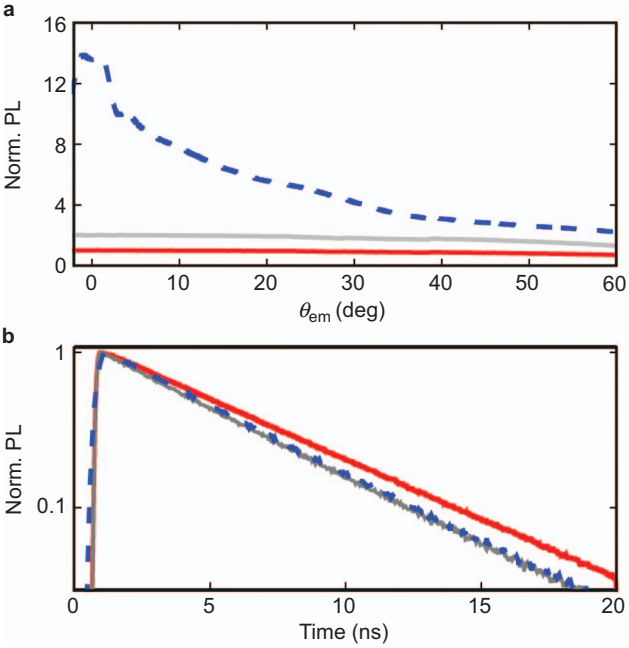

Figure 4 (**a**) Integrated PL between 1.75 eV and 2.15 eV, measured as a function of the emission angle from the emitting layer deposited on top of a flat dielectric substrate (solid red curve), from a similar layer on top of the periodic array of aluminum particles (dashed blue curve) and on top of aluminum particles arranged in a disordered lattice (solid gray curve). These results are normalized by the PL integrated into the same spectral range and measured from the dye layer deposited on top of a flat dielectric substrate at θ_{em}=0°. (**b**) Normalized luminescence decay measured from the emitting layer deposited on top of a flat dielectric substrate (solid red curve), of the periodic array of aluminum particles (dashed blue curve) and of the aluminum particles arranged in a random fashion (solid gray curve). The decays are single-exponential with a decay rate of γ=0.18 ns^{-1} for the flat dielectric substrate and γ=0.21 ns^{-1} for both the periodic and random arrays. PL, photoluminescence.

evaluated.[43] The results for the unpolarized emission are displayed in Figure 3b. The number of bands obtained from the simulation, their spectral positions, the dispersion and the PLDE values are in good agreement with the measurements. In Figure 3c, we present numerical simulations that do not consider any resonant enhancement at the pump frequency, providing a maximum enhancement of ~12 times.

To examine the angular modification of the emission by the plasmonic structure in more detail, in Figure 4a, we present the PL integrated throughout the emission spectrum of the dye (between 1.75 eV and 2.15 eV), normalized by the integrated PL measured from a planar polymer/dye structure of the same thickness at θ_{em}=0°. We compare the angular distribution of the emission measured from the plasmonic (dashed blue curve) to the planar (solid red curve) structures. The emission of the planar sample resembles a Lambertian radiator. However, the plasmonic structure significantly enhances the emission within a narrow angular window, demonstrating the beaming of the emitted light. The integrated directional enhancement over the emission spectrum reaches a factor of 14 in the forward direction. SLRs extend laterally over several unit cells of the array and extend for distances of several microns.[32] Therefore, coupling emitters to SLRs yields a source with an increased spatial coherence: the emission from single dye molecules couples to surface modes in the particle array, which becomes the emission coupled out by the array and interferes constructively in the forward direction.

We have performed extinction and PLDE experiments on a random array of aluminum particles with the same particle density as the periodic array (see Supplementary Information). The emitter layer and the particle dimensions are the same, but because of the lack of periodicity, the random array sustains localized surface plasmon polaritons in the individual particles but not extended SLRs.[44] The solid gray curve in Figure 4a represents the angular dependence of the PL integrated throughout the emission range and normalized to the emission of the polymer/dye layer at θ_{em}=0°. We observe only a twofold emission enhancement, primarily because of the increased scattering of the blue pump. The emission of the random array shows a Lambertian dependence. These measurements demonstrate the large impact that periodicity in the particle array exerts on the directional enhancement of the emission. The twofold integrated enhancement is seven times lower than that obtained from the periodic structure close to the forward direction, indicating the stronger effect of collective SLRs versus localized resonances in the modification of the emission.

To complete the description of the modified emission coupled to nanoparticle arrays, we have determined the decay rate of dye molecules covering plasmonic arrays of particles. Figure 4b displays the time-resolved fluorescence of a layer with the same concentration and the same thickness but deposited on a dielectric substrate (solid red curve), the ordered particle array (dashed blue curve) and the disordered array (solid gray curve). By comparing the dashed blue and solid gray curves in Figure 4b, it is clear that a nearly identical decay rate enhancement is present independently of the particle ordering, compared to the dye-doped polymer layer without metallic particles. According to the classification of light sources provided in Ref.

45, the dye molecules employed in our investigation can be considered as constant power sources because of their very high QE. Constant power sources are not influenced by a change in the LDOS, and the total emitted power scales linearly with the total absorbed power. For this reason, the total decay rate enhancement experimentally observed may be attributed to a non-radiative decay channel introduced by the metal rather than by the SLRs in the array. It has been argued that because the presence of metallic particles near emitters introduces a non-radiative decay channel,[38,39] the primary effect on the high QE emitters is the reduction of their efficiency.[34–36] Therefore, the observed decay-rate enhancement can be attributed to the quenching of the emission. This quenching is considered a major drawback in realistic applications. However, our decay-rate measurements show a reduction in QE of only 15% but a maximum 60-fold and an integrated 14-fold directional enhancement in the forward emission direction. Based on these results, we infer that the maximum ~60-fold directional enhancement measured for the unpolarized emission may be approximately expressed as the product of a factor of ~6 due to pump enhancement and a factor of ~10 due to emission enhancement.

Having discussed how plasmonic structures can boost the performance of a thin layer of luminescent material, we take a step forward toward their integration into SSL applications. Figure 5a displays the emission characteristics of the plasmonic structure when pumping with a standard high-power Lambertian-like blue LED. The main difference between the measurements presented in Figures 2a and 5a is found on the excitation source, i.e., the LED has a shorter coherence length and a broader angular radiation pattern than the laser. Regardless of the excitation source, it is observed that the features in the PLDE dispersion diagram remain unaffected because they are determined by the dispersion of the SLRs at the emission energies. However, the total enhancement factor is lower for the case of the LED excitation because of the non-collimated illumination of the nanoparticle array, which leads to the less efficient pump enhancement of the dye and, therefore, a lower integrated PLDE. Figure 5b displays the angular dependence of the PLDE measured at 2.01 eV. In spite of the lower emission enhancement achieved using LED illumination, the PLDE reaches a factor of 20 in the forward direction. These results further support the integration of plasmonics into lighting applications that require control over the directionality of the emission. The plasmonic antenna array acts as efficient integrated optics for the beam collimation.

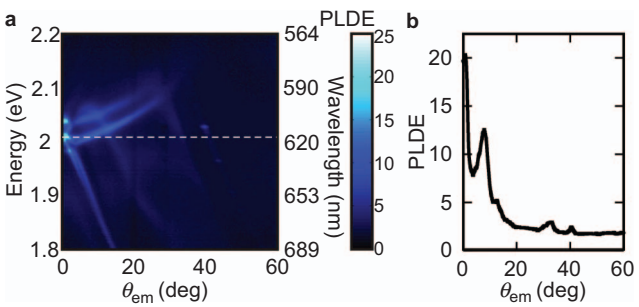

Figure 5 (**a**) PLDE spectra of a layer of dye molecules on top of an array of Al antennas as a function of the emission angle, θ_{em}, obtained by exciting the dye with a blue LED. (**b**) PLDE versus θ_{em} at 2.01 eV. LED, light-emitting diode; PLDE, photoluminescence directional enhancement.

CONCLUSIONS

In summary, we have demonstrated that plasmonics provides a reliable platform for state-of-the-art lighting applications. We have fabricated a large-area periodic array of aluminum particles or nanoantennas using an imprint lithography technique. This array significantly increases the emission of a layer of high-QE dye molecules deposited on top. The enhancement of the unpolarized emission reaches a factor of 60 at certain frequencies in the forward direction and a factor of 14 when integrated over the entire emission range. The emission's directional enhancement is explained as a combination of the resonant excitation of the emitters and the enhancement of their spatial coherence, which leads to a highly directional emission. This behavior is the result of the emission of the dye into collective plasmonic resonances that result from the coupling of localized surface plasmon polaritons to diffracted orders in the array. Collective resonances or surface lattice resonances have a large spatial extension, enhancing the emission in defined directions. In addition, we have investigated the combination of these structures with high-power standard blue LED sources, showing that the plasmonic structure acts as an integrated optical component to shape the emission pattern of the dye layer. The combination of plasmonics and LEDs will pave the way for a new generation of SSL devices, as the appropriate design of the array will allow us to tailor the directionality, polarization and color of the emission with unprecedented accuracy.

ACKNOWLEDGMENTS

This work is part of the research program of the Foundation for Fundamental Research on Matter (FOM), which is financially supported by the Netherlands Organization for Fundamental Research (NWO). It is also part of an industrial partnership program between Philips and FOM. It is supported by NanoNextNL of the Government of the Netherlands and 130 partners. SM is grateful for the Young Researcher Overseas Visits Program for Vitalizing Brain Circulation of JSPS, Japan.

1 Pimputkar S, Speck JS, DenBaars SP, Nakamura S. Prospects for LED lighting. *Nat Photon* 2009; **3**: 180–182.
2 Kido J, Kimura M, Nagai K. Multilayer white light-emitting organic electroluminescent device. *Science* 1995; **267**: 1332–1334.
3 Phillips JM, Coltrin ME, Crawford MH, Fischer AJ, Krames MR *et al*. Research challenges to ultra-efficient inorganic solid-state lighting. *Laser Photon Rev* 2007; **1**: 307–333.
4 Schlotter P, Schmidt R, Schneider J. Luminescence conversion of blue light emitting diodes. *J Appl Phys A* 1997; **64**: 417–418.
5 Reineke S, Lindner F, Schwartz G, Seidler N, Walzer K *et al*. White organic light-emitting diodes with fluorescent tube efficiency. *Nature* 2009; **459**: 234–238.
6 Wierer JJ, David A, Megens MM. III-nitride photonic-crystal light-emitting diodes with high extraction efficiency. *Nat Photon* 2009; **3**: 163–169.
7 Greffet JJ. Nanoantennas for light emission. *Science* 2005; **308**: 1561.
8 Eisler HJ, Martin OJ, Hecht B, Pohl DW. Resonant optical antennas. *Science* 2005; **308**: 1607–1609.
9 Bharadwaj P, Deutsch B, Novotny L. Optical antennas. *Adv Opt Photon* 2009; **1**: 438–483.
10 Giannini V, Fernández-Domínguez AI, Heck SC, Maier SA. Plasmonic nanoantennas: fundamentals and their use in controlling the radiative properties of nanoemitters. *Chem Rev* 2011; **111**: 3888–3912.
11 Novotny L, van Hulst N. Antennas for light. *Nat Photon* 2011; **5**: 83–90.
12 Alaverdyan Y, Sepúlveda B, Eurenius L, Olsson E, Käll M. Optical antennas based on coupled nanoholes in thin metal films. *Nat Phys* 2007; **3**: 884–889.
13 Polman A. Plasmonics applied. *Science* 2008; **332**: 868–869.
14 Aouani H, Mahboub O, Bonod N, Devaux E, Popov E *et al*. Bright unidirectional fluorescence emission of molecules in a nanoaperture with plasmonic corrugations. *Nano Lett* 2011; **11**: 637–644.
15 Song JH, Atay T, Shi S, Urabe H, Nurmikko AV. Large enhancement of fluorescence efficiency from CdSe/ZnS quantum dots induced by resonant coupling to spatially controlled surface plasmons. *Nano Lett* 2005; **5**: 1557–1561.
16 Tam F, Goodrich GP, Johnson BR, Halas NJ. Plasmonic enhancement of molecular fluorescence. *Nano Lett* 2007; **7**: 496–501.

doi:10.1038/lsa.2013.22

17 Kinkhabwala A, Yu ZF, Fan SH, Avlasevich T, Mullen K *et al*. Large single-molecule fluorescence enhancements produced by a bowtie nanoantenna. *Nat Photon* 2009; **3**: 654–657.
18 Giannini V, Sánchez-Gil JA, Muskens O, Gómez Rivas J. Electrodynamic calculations of spontaneous emission coupled to metal nanostructures of arbitrary shape: nanoantenna-enhanced fluorescence. *J Opt Soc Am B* 2009; **26**: 1569–1577.
19 Bharadwaj P, Novotny L. Plasmon-enhanced photoemission from a single $Y_3N@C_{80}$ fullerene. *J Phys Chem C* 2010; **114**: 7444–7447.
20 Khurgin JB, Sun G, Soref RA. Enhancement of luminescence efficiency using surface plasmon polaritons: figures of merit. *J Opt Soc Am B* 2007; **24**: 1968–1980.
21 Mertens H, Polman, A. Strong luminescence quantum-efficiency enhancement near prolate metal nanoparticles: dipolar versus higher-order modes. *J Appl Phys* 2009; **105**: 044302.
22 Wenger J. Fluorescence enhancement factors on optical antennas: enlarging the experimental values without changing the antenna design. *Int J Opt* 2012; **2012**: 828121.
23 Sun G, Khurgin JB, Soref RA. Plasmonic light-emission enhancement with isolated metal nanoparticles and their coupled arrays. *J Opt Soc Am B* 2008; **25**: 1748–1755.
24 Geiger C, Fick J. Surface plasmon-mediated far-field emission of laser dye solutions. *Opt Lett* 2010; **35**: 2245–2247.
25 Verschuuren MA. Substrate Conformal Imprint Lithographhy for Nanophotonics. PhD thesis, Utrecht University, Utrecht, The Netherlands, 2010.
26 Spinelli P, Verschuuren MA, Polman A. Broadband omnidirectional antireflection coating based on subwavelength surface Mie resonators. *Nat Comm* 2012; **3**: 692.
27 García de Abajo F, Sáenz JJ. Electromagnetic surface modes in structured perfect-conductor surfaces. *Phys Rev Lett* 2005; **95**: 233901.
28 Kravets VG, Schedin F, Grigorenko AN. Extremely narrow plasmon resonances based on diffraction coupling of localized plasmons in arrays of metallic nanoparticles. *Phys Rev Lett* 2008; **101**: 087403.
29 Auguié, B, Barnes WL. Collective resonances in gold nanoparticle arrays. *Phys Rev Lett* 2008; **101**: 143902.
30 Chu Y, Schonbrun E, Yang T, Crozier KB. Experimental observation of narrow surface plasmon resonances in gold nanoparticle arrays. *Appl Phys Lett* 2008; **93**: 181108.
31 Vecchi G, Giannini V, Gómez Rivas J. Shaping the fluorescent emission by lattice resonances in plasmonic crystals of nanoantennas. *Phys Rev Lett* 2009; **102**: 146807.
32 Zhou W, Odom TW. Tunable subradiant lattice plasmons by out-of-plane dipolar interactions. *Nat Nanotech* 2011; **6**: 423–427.
33 Rodríguez SR, Lozano G, Verschuuren MA, Gomes R, Lambert K *et al*. Quantum rod emission coupled to plasmonic lattice resonances: a collective directional source of polarized light. *Appl Phys Lett* 2012; **100**: 111103.
34 Vecchi G, Giannini V, Gómez Rivas J. Surface modes in plasmonic crystals induced by diffractive coupling of nanoantennas. *Phys Rev B* 2009; **80**: 201401.
35 Pellegrini G, Mattei G. Mazzoldi P. Nanoantenna arrays for large-area emission enhancement. *J Phys Chem C* 2011; **115**: 24662–24665.
36 Pellegrini G, Mattei G, Mazzoldi P. Light extraction with dielectric nanoantenna arrays. *ACS Nano* 2009; **3**: 2715–2721.
37 Bakker RM, Drachev VP, Liu Z, Yuan HK, Pedersen RH *et al*. Nanoantenna array-induced fluorescence enhancement and reduced lifetimes. *New J Phys* 2008; **10**: 125022.
38 Sun G, Khurgin JB, Soref RA. Practical enhancement of photoluminescence by metal nanoparticles. *Appl Phys Lett* 2009; **94**: 101103.
39 Rogobete L, Kaminski F, Agio M, Sandoghar V. Design of plasmonic nanoantennae for enhancing spontaneous emission. *Opt Lett* 2007; **32**: 1623–1625.
40 Kim JK, Luo H, Schubert EF, Cho J, Sone C *et al*. Strongly enhanced phosphor efficiency in GaInN white light-emitting diodes using remote phosphor configuration and diffuse reflector cup. *Jpn J Appl Phys* 2005; **44**: 649–651.
41 Anger P, Bharadwaj P, Novotny L. Enhancement and quenching of single-molecule fluorescence. *Phys Rev Lett* 2006; **96**: 113002.
42 Kühn S, Hakanson U, Rogobete L, Sandoghdar V. Enhancement of single-molecule fluorescence using a gold nanoparticle as an optical nanoantenna. *Phys Rev Lett* 2006; **97**: 017402.
43 Lalanne P, Besbes M, Hugonin JP, van Haver S, Janssen OT *et al*. Numerical analysis of a slit-groove diffraction problem. *J Eur Opt Soc Rap Pub* 2007; **2**: 07022.
44 Auguié B, Barnes WL. Diffractive coupling in gold nanoparticle arrays and the effect of disorder. *Opt Lett* 2009; **34**: 401–403.
45 El-Dardiry RG, Faez S, Lagendijk A. Classification of light sources and their interaction with active and passive environments. *Phys Rev A* 2011; **83**: 031801.

Supplementary Information for this article can be found on *Light: Science & Applications*' website (http://www.nature.com/lsa/).

Plasmonics for solid-state lighting: Enhanced excitation and directional emission of highly efficient light sources

Gabriel Lozano[1,*], Davy J. Louwers[2], Said R. K. Rodríguez[1], Shunsuke Murai[1,3], Olaf T. A. Jansen,[2] Marc A. Verschuuren[2] and Jaime Gómez Rivas[1,4,*]

[1]Center for Nanophotonics, FOM Institute AMOLF, c/o Philips Research Laboratories, Eindhoven, The Netherlands
[2]Philips Research Laboratories, Eindhoven, The Netherlands
[3]Department of Material Chemistry, Graduate School of Engineering, Kyoto University, Kyoto, Japan
[4]COBRA Research Institute, Eindhoven University of Technology, Eindhoven, The Netherlands

*To whom correspondence should be addressed: Dr. G. Lozano, Email: lozano@amolf.nl and Prof. J. Gómez-Rivas, email: rivas@amolf.nl, High Tech Campus 4, 5656 AE, Eindhoven, The Netherlands, Tel: +31(0) 402742349, Fax: +31(0) 402746505

SUPPLEMENTARY INFORMATION

In Fig. S1a we present the variable angle extinction spectra of the periodic array of aluminum nanoparticles as a function of the incident angle for s-polarized light. The color curves indicate the onset of diffraction, the so-called Rayleigh anomalies (RAs), of beams diffracted by the array of aluminum particles. The RAs correspond to the condition at which diffracted orders are grazing to the surface of the array. These RAs are calculated taking 1.47, 1.52 or 1.55 as the refractive index of the diffraction medium. The narrow bands of high extinction follow the dispersion of the RAs. The origin of these resonances, known as surface lattice resonances (SLRs), resides in the diffractive coupling of localized surface plasmon polaritons supported by the individual particles. Figure S1b displays the PLDE dispersion diagram for s-polarized emission. The bands of high photoluminescence directional enhancement (PLDE) correspond to SLRs supported by the array observed in extinction.

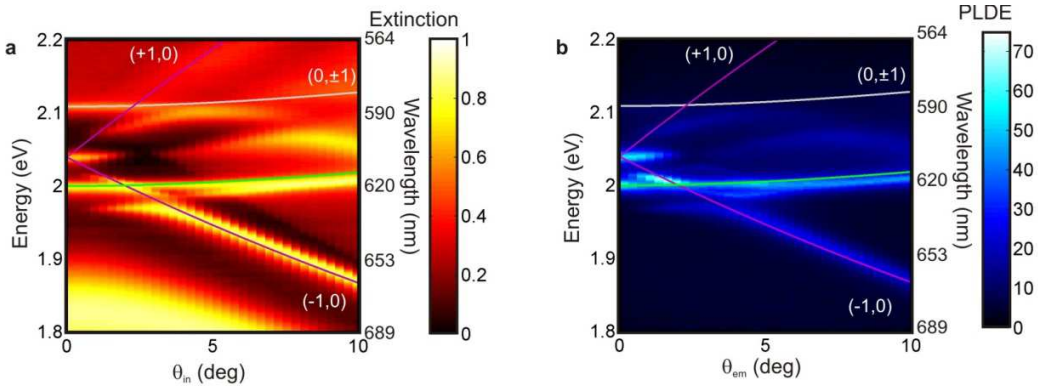

Fig. S1. **a** Extinction of s-polarized light as a function of the photon energy and the angle of incidence θ_{in} of a layer of dye deposited on top of an array of aluminum antennas. **b** s-polarized PLDE as a function of the photon energy and the emission angle θ_{em} measured from the same structure excited with a 2.76 eV

continuous wave laser at θ_{ex}=0 deg. Grey, purple and green curves correspond to the Raleigh anomalies calculated for the beams diffracted in a medium with refractive index 1.47, 1.52 and 1.55, respectively.

Figs. S2, S3, S4 and S5 show FDTD simulations in a plasmonic array of particles covered by a polymer layer. Fig. S2a shows the comparison between measured (black curve) and simulated extinction (grey curve) at θ_{in}=0 deg. The extinction spectra displayed in Fig. S2a show four distinct resonances with different line-widths. On the one hand, one broad resonance is observed at 1.85 eV. On the other, three narrow peaks located at 2.00 eV, 2.04 eV and 2.11 eV stand out. In order to shed light in the origin and field distribution of these resonances, we have performed FDTD simulations on the spatial distribution of the electric field intensity enhancement, i.e. near field intensity normalized by the incident intensity. Results are shown in Figs. S2b-e. Fig. S2b shows the field profile for the broad resonance displayed at 1.85 eV. A high intensity enhancement close to the particles is observed, confirming that this resonance is associated to the excitation of a localized plasmon resonance in the nanoparticles. In contrast, for 2 eV, 2.04 eV and 2.11 eV the field enhancements extend over a large volume around the particles as it is shown in Fig. S2c, S2d and S2e, respectively. These three narrow peaks are associated to the excitation of quasi-bonded surface modes on collective modes supported by the array of aluminum particles. These modes result from the diffractive coupling of localized surface plasmon polaritons. By comparing the different field profiles, it is possible to conclude that the different refractive index layers surrounding the array and the finite thickness of the polystyrene layer have a large impact on the field enhancement distribution. In particular, for 2.11 eV the field extends more into the lower medium, i.e., substrate, than for 2.04 eV and 2.00 eV, leading to a lower effective refractive index for this mode and therefore to a shift of the resonance towards higher energies. Figure S3 shows the spatial distribution of the field intensity enhancement on a plane intersecting the antennas at y=D/2 in a unit cell of the array. The cut presented in S2b does not show the highest values of the near field which are observed nearby the corners of the metallic particle as it is displayed in Fig. S3a. However, it is noteworthy to mention that the electric field enhancement calculated in a particular plane and the extinction of the system should not be compared quantitatively. Specifically, extinction is a far-field magnitude representing the amount of light removed from the forwardly transmitted beam whereas the electric field enhancement is a near-field quantity. Figure S4 shows the dipolar character of the localized surface plasmon resonance observed in extinction at normal incidence and 1.85 eV. Simulations of the total electric field enhancement in a plane intersecting the antennas in their middle height (z=h/2) are shown in Fig. S4. It is considered a plane wave with photon energy 1.85 eV illuminating the array at normal incidence. The field is mostly enhanced at the edges of the nanoantennas displaying a dipolar-like radiation pattern. In Fig. S5, the spatial distribution of the intensity enhancement in a plane parallel to the array at z=270 nm, i.e. within the polymer layer, is presented. It should be noted that only for the 2 eV and 2.04 eV modes the field intensity is significantly enhanced, leading to the large PLDE values experimentally observed.

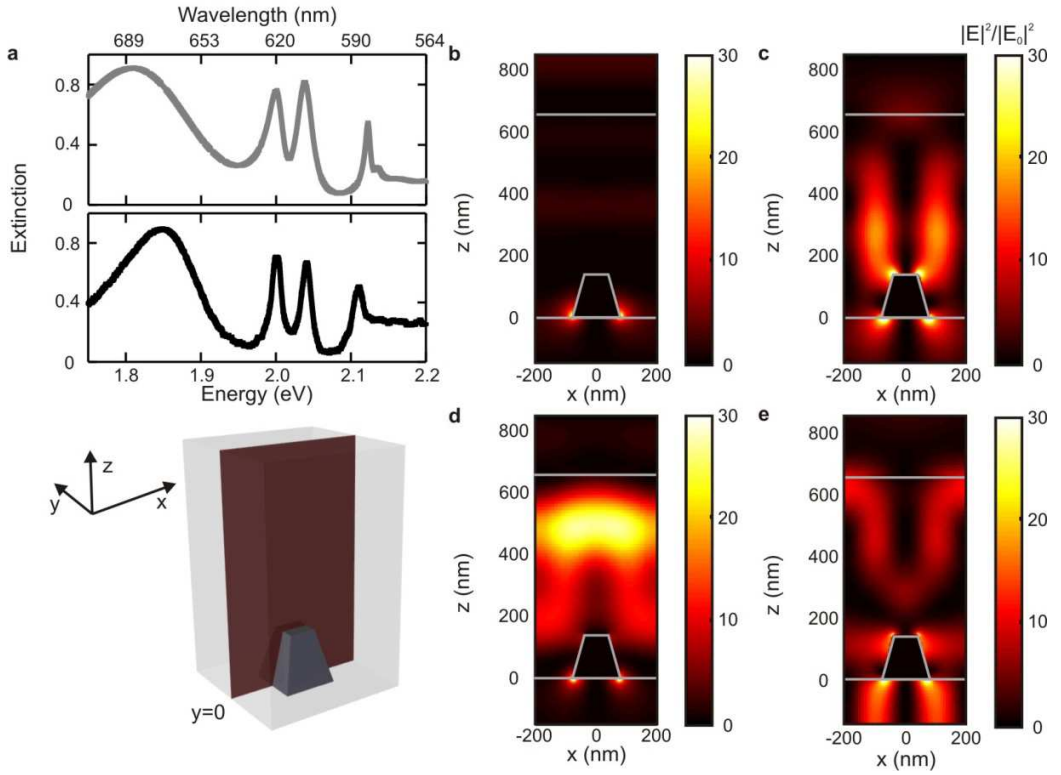

Fig. S2. **a** Measured (black curve, lower panel) and three dimensional FDTD simulated extinction (grey curve, upper panel) spectra at θ_{in}=0 deg of an array of aluminum particles on fused silica covered by a 650 nm thick layer of refractive index 1.59. **b-e** Spatial distribution of the local field intensity enhancement simulated in the same structure. Simulations consider a plane wave incident normal to the array with photon energy **b** 1.85 eV, **c** 2 eV, **d** 2.04 eV and **e** 2.11 eV. The colour plot indicates the intensity enhancement on the plane intersecting the antennas at y=0 in a unit cell of the array. The sketch shows the plane along which the field distributions are calculated. The antenna and the different dielectric interfaces are outlined using grey curves.

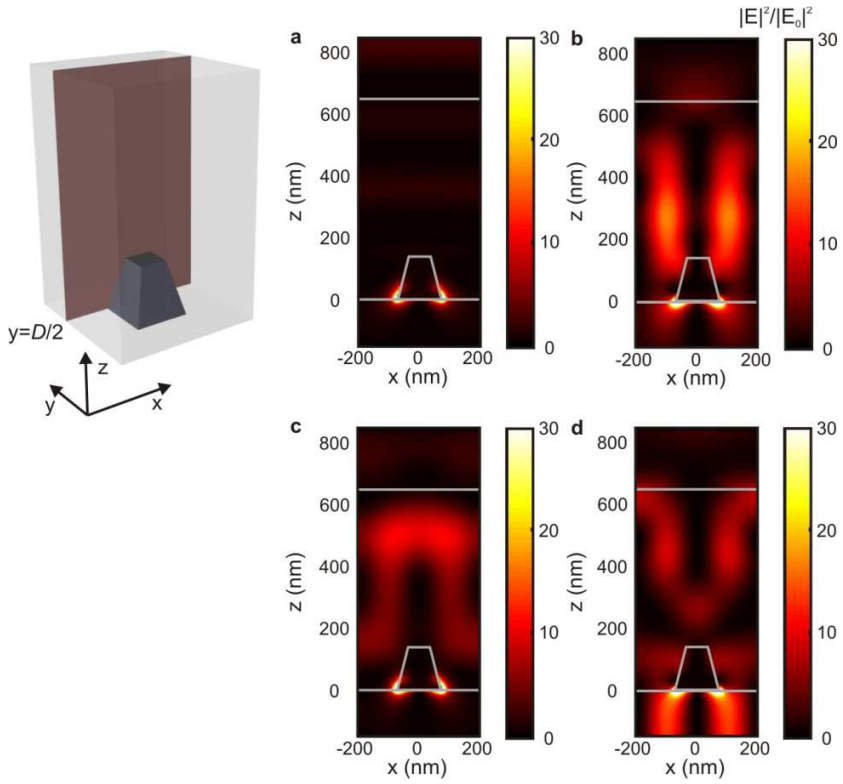

Fig. S3. Spatial distribution of the electric field intensity enhancement simulated in the same structure of Fig S2. Simulations consider a plane wave incident normal to the array with photon energy **a** 1.85 eV, **b** 2 eV, **c** 2.04 eV and **d** 2.11 eV. The colour plot indicates the intensity enhancement on the plane intersecting the antennas at y=*D*/2 in a unit cell of the array. The sketch shows the plane along which the field distributions are calculated. The antenna and the different dielectric interfaces are outlined using grey curves.

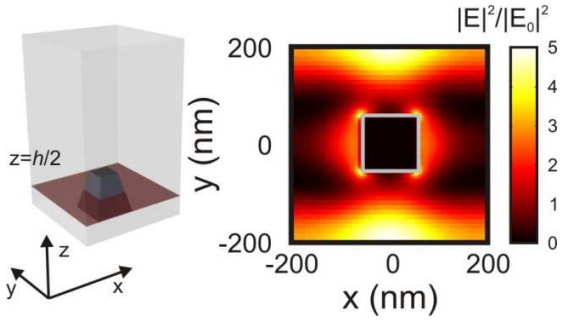

Fig. S4. Spatial distribution of the electric field intensity enhancement simulated in the same structure of Fig. S2. Simulations consider a plane wave incident normal to the array with photon energy 1.85 eV. The colour plot indicates the intensity enhancement on a plane parallel to the array at z=*h*/2 in a unit cell of the array. The sketch shows the plane along which the field distributions is calculated. The antenna is outlined using a grey curve.

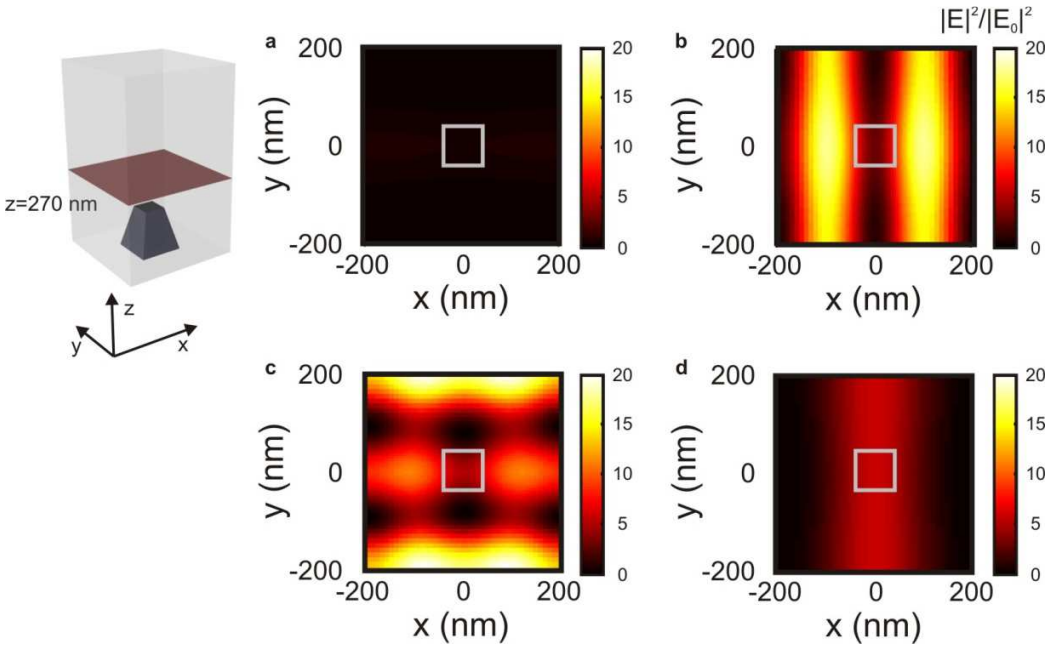

Fig. S5. Spatial distribution of the electric field intensity enhancement simulated in the same structure of Fig. S2. Simulations consider a plane wave incident normal to the array with photon energy **a** 1.85 eV, **b** 2 eV, **c** 2.04 eV and **d** 2.11 eV. The colour plot indicates the intensity enhancement on a plane parallel to the array at z=270 nm in a unit cell of the array. The sketch shows the plane along which the field distributions are calculated. The antenna is outlined using a grey curve.

In Figure S6, we display the PLE spectra as a function of θ_{em} for a broad angular range when the dye molecules are excited at θ_{ex}=0 deg and at θ_{ex}=10 deg. The comparison shows that the dispersive characteristics of the PLDE remain unaltered when θ_{ex} is varied because the directionality in the emission is determined by the resonances at the emission frequencies. However, the overall enhancement is reduced by a factor of two between θ_{ex}=0 and θ_{ex}=10 deg due to the reduction of the pump enhancement. To further illustrate the origin of this difference, in Fig. S7 we present the extinction of the excitation light (2.76 eV) as a function of the incident angle, showing a strong correlation between the amount of blue light transmitted through the sample and the integrated PLDE. At θ_{in}=0 deg the extinction is significantly higher than at θ_{in}=10 deg, indicating that for this frequency and the angle of incidence the nanoparticle array is resonant. This is attributed to the (-1,1) SLR. This resonant behavior leads to the more efficient excitation of the dye and the higher PLE at θ_{ex}=0 deg compared to θ_{ex}=10 deg.

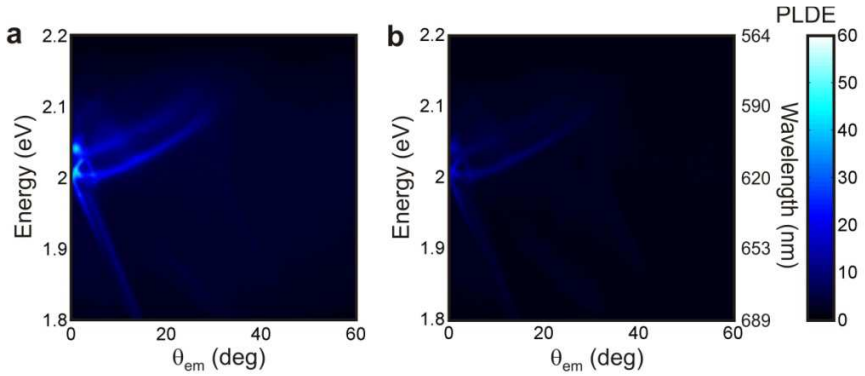

Fig. S6. PLDE as a function of the photon energy and the emission angle, θ_{em}, measured from an emitting layer deposited on top of a plasmonic structure when pumping with a 2.76 eV continuous wave laser at **a** θ_{ex}=0 deg and **b** θ_{ex}=10 deg.

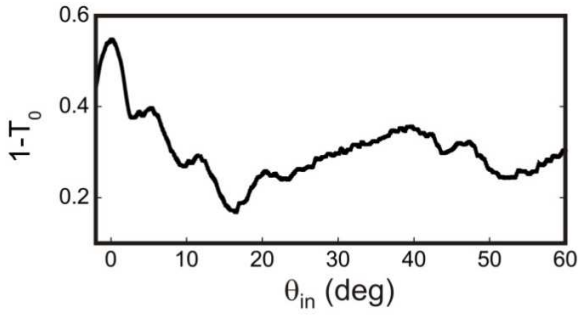

Fig. S7. Extinction spectrum of the periodic array of aluminum nanoantennas measured at 2.76 eV as a function of the angle of incidence, θ_{in}.

To clarify the influence of the periodicity in the plasmonic structure on the PL enhancement, we have deposited a dye layer with the same concentration and the same thickness on top of a random array of similar nanoantennas. A SEM picture of such array is shown as an inset in Fig. S8a. This random array supports localized surface plasmon polaritons but not SLRs. In Figs. S8a-b we show extinction and PLDE measurements as a function of θ_{in} and θ_{em}, respectively. We find a comparable enhancement factor (~3) for the random and the periodic array when measuring the PL far from any SLR, i.e. at θ_{em}=50 deg or at θ_{em}=0 and 1.85 eV. However, this value is much lower than the maximum measured for the periodic array close to the forward direction.

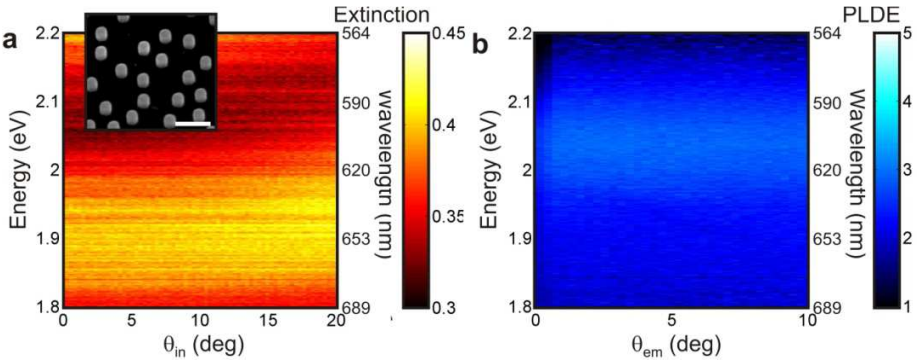

Fig. S8. **a** Extinction of unpolarized light as a function of the photon energy and the angle of incidence, θ_{in}, measured from a layer of light emitters deposited on top of an array of metallic particles randomly arranged. Inset: SEM picture of such random array. Scale bar indicates 500 nm. **b** Unpolarized PLDE as a function of the photon energy and the angle of emission, θ_{em}, measured from the same structure when pumping with a 2.76 eV continous wave laser at θ_{ex}=0 deg.

Prior to the life time measurements of the dye on plasmonic structures, the concentration quenching effect on the decay rate was studied. Figure S9 displays the fitted decay rates as a function of dye concentration in polystyrene. We find significant concentration quenching effects when the fraction of dye in the polymer is above 5 wt%.

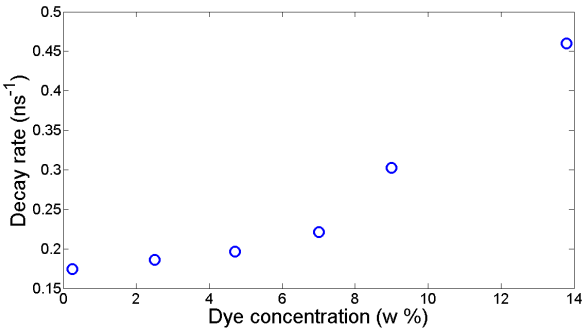

Fig. S9. Total decay rate of excited dye molecules as a function of the weight fraction of dye present in the polymer matrix.

We have also measured variable angle extinction (see Fig. S10a) and emission spectra (see Fig. S10b) from a polymer layer doped with the same die but deposited on top of an array of similar antennas in which the LSPR is blue shifted respect to the measurements shown in Fig. 2a. The spectral position of the LSPR overlaps with the maximum of dye emission for this geometry, leading to a similar PLDE factor. In either case, the improvement associated to localized plasmon resonances is far lower than the one attained from the periodic structure close to the forward direction.

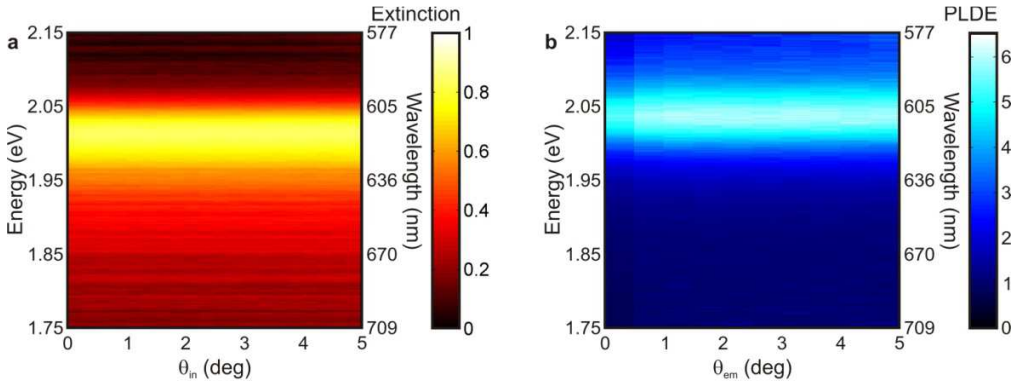

Fig. S10. Extinction of p-polarized light as a function of the photon energy and the angle of incidence θ_{in} of a layer of dye deposited on top of an array of aluminum antennas. **b** p-polarized PLDE as a function of the photon energy and the emission angle θ_{em} measured on the same structure excited with a 450 nm continuous wave laser at θ_{ex}=0 deg.